Physiol Genomics 7: 201–213, 2001.
First published November 15, 2001; 10.1152/physiolgenomics.00074.2001.

Gene expression profiling of acute spinal cord injury reveals spreading inflammatory signals and neuron loss

JASON B. CARMEL,[1] ANTHONY GALANTE,[3] PATRICIA SOTEROPOULOS,[3] PETER TOLIAS,[3] MICHAEL RECCE,[4] WISE YOUNG,[1] AND RONALD P. HART[1,2]

[1]*W. M. Keck Center for Collaborative Neuroscience, Rutgers University, Piscataway 08854;* [2]*Department of Biological Sciences, Rutgers University, Newark, NJ 07102;* [3]*Center for Applied Genomics, Public Health Research Institute and University of Medicine and Dentistry of New Jersey, New Jersey Medical School, Newark 07103; and* [4]*Center for Computational Biology and Bioengineering, New Jersey Institute of Technology, Newark, New Jersey 07103*

Received 4 September 2001; accepted in final form 7 November 2001

Carmel, Jason B., Anthony Galante, Patricia Soteropoulos, Peter Tolias, Michael Recce, Wise Young, and Ronald P. Hart. Gene expression profiling of acute spinal cord injury reveals spreading inflammatory signals and neuron loss. *Physiol Genomics* 7: 201–213, 2001. First published November 15, 2001; 10.1152/physiolgenomics.00074.2001.—We have completed the first large-scale gene expression study of acute spinal cord injury (SCI) in rat. Oligonucleotide microarrays containing 1,200 gene-specific probes were used to quantify mRNA levels, relative to uninjured controls, in spinal cords injured using a standard contusion model. Our results revealed a marked loss of neuron-specific mRNAs at the injury site. The surviving cells showed a characteristic inflammatory response that started at the injury site and spread to the distal cord. Changes in several mRNA levels were associated with putative regenerative responses in the spinal cord. Notably, phosphodiesterase 4, nestin, glia-derived neurite promoting factor, and GAP-43 mRNAs increased significantly. Other mRNAs clustered temporally and spatially with these regeneration-associated genes. Thus we have described global patterns of gene expression following acute SCI, and we have identified targets for future study and possible therapeutic intervention.

spinal cord injury; microarray; gene expression; regeneration-associated genes; inflammation; cell death

CONTUSION OF SPINAL CORD TISSUE leads to a rapid destruction of cells at the site of injury, an intense inflammatory response, secondary necrotic and apoptotic cell death, and reparative responses. These responses to injury are likely to be mediated and reflected by changes in mRNA concentrations, regardless of whether these changes are due to regulated gene expression or to altered cellular populations. Many investigators have measured the expression of individual genes in injured spinal cords, particularly genes involved with inflammation (1, 21, 34, 42, 45, 49, 52, 53), apoptosis (11, 33, 39, 41), excitotoxicity (19, 20), and neurotrophin stimulation (21, 29, 41). None, however, has measured large numbers of genes and their temporal and spatial relationships. We used oligonucleotide-based microarrays (10, 30, 31) to measure the mRNA levels of 1,200 representative genes implicated in major rat central nervous system (CNS) functions. Many studies have proved the utility of this approach in other systems, including Alzheimer's disease (23), schizophrenia (36), auditory plasticity (32), and multiple sclerosis (50).

We had three goals in this study. First, we sought to define the temporal and spatial distribution of mRNA changes following acute spinal cord injury (SCI). By clustering genes with similar expression patterns, we hoped to discover mRNA changes that predict or explain cellular and tissue responses to injury. Second, we wished to identify genes that had not previously been studied in SCI and whose pattern of expression would make them good targets for future investigation. Finally, we wanted to create a database that can be used to compare gene expression changes due to pharmacological or cellular therapies.

MATERIALS AND METHODS

Surgery. Twenty-four Long-Evans rats were injured using the MASCIS impactor (Multi-Center Animal Spinal Cord Injury Study, formerly known as the NYU impactor; Ref. 12). Rats were anesthetized with intraperitoneal pentobarbital (45 mg/kg for females, 65 mg/kg for males) and then contused by dropping a 10-g rod a distance of 25 mm onto T9–10 spinal cord exposed by laminectomy. An additional seven rats served as uninjured controls. Rats were injured and treated without regard to sex, and groups differed in numbers and ratio of males and females. For the composition of the groups by numbers and sex of the animals, please refer to the

Article published online before print. See web site for date of publication (http://physiolgenomics.physiology.org).

Address for reprint requests and other correspondence: R. P. Hart, W. M. Keck Center for Collaborative Neuroscience, Rutgers Univ., 604 Allison Rd. Rm. D251, Piscataway, NJ 08854 (rhart@andromeda.rutgers.edu).

The costs of publication of this article were defrayed in part by the payment of page charges. The article must therefore be hereby marked "*advertisement*" in accordance with 18 U.S.C. Section 1734 solely to indicate this fact.

Supplementary Material[1] for this article, published online at the *Physiological Genomics* web site; also, a complete table of results, in the form of a searchable database, is available at **http://spine.rutgers.edu/microarray**. At 6, 12, 24, or 48 h after injury, rats were anesthetized with pentobarbital. Their spinal columns were rapidly removed to ice for dissection, and the spinal cord was immediately placed on a bed of dry ice. A 5-mm segment of spinal cord centered on the point of impact was collected and labeled "I" for injury site. The adjacent 5-mm segment distal to the impact segment was collected and labeled "D1." Segments were frozen at −80°C until RNA preparation.

Atomic absorption spectroscopy. We used atomic absorption values as correlates of lesion volume. Potassium measurements were made on a separate set of animals (n = 4 at each time point; 2 male and 2 female) using identical injury methods. Tissues were weighed to obtain the wet weight before homogenization in Trizol (Invitrogen) to extract RNA (see below). Trizol contains sodium but no potassium, so potassium alone was used to determine lesion volume. Although our lab has historically used both potassium and sodium to measure lesion volume, potassium itself correlates with injury severity (26) and is a precise measure of lesion volume. An aliquot of the Trizol homogenate was removed and diluted in water for atomic absorption spectroscopy to measure potassium using a Perkin-Elmer model 3100 spectrometer. Results were expressed as micromoles of potassium per gram of tissue.

Target preparation. Total cellular RNA was prepared from Trizol homogenates as recommended by the manufacturer, followed by precipitation with 2 M ammonium acetate and ethanol. Ultraviolet absorbance spectroscopy was used to measure the concentration and purity of the resulting RNA. Approximately 10 μg of total RNA was used for each target. Depending on the quantity of RNA recovered from each tissue segment, RNA was pooled from 1–3 animals. Each 10-μg sample constitutes one of three independent replicate groups at each time point. RNA was reverse-transcribed into double-stranded cDNA with a T_7 promoter-containing primer using Superscript II (Invitrogen Life Technologies), as recommended by Affymetrix. Following extraction with phenol-chloroform and ethanol precipitation from ammonium acetate, the cDNA was used as a template in a biotin-labeled in vitro transcription reaction (Enzo BioArray, Affymetrix). Resulting target cRNA was collected on RNeasy columns (Qiagen) and then fragmented for hybridization to the microarrays.

Microarrays. The rat neurobiology U34 microarray from Affymetrix was used in all hybridizations. This array contains a 1,200-gene set chosen to represent important CNS functions. Probes consist of 16 pairs of 25-mer oligonucleotides. One member of each pair contains a point mutation, and the signals of the pair are compared to assess specificity of hybridization. Biotinylated target cDNA was hybridized onto the array and then processed using the Affymetrix GeneChip Fluidics Workstation 400, following the Mini_Euk 2v2 protocol, except that only 3 μg of fragmented cRNA was added to the hybridization cocktail. Following binding with phycoerythrin-coupled avidin, microarrays were scanned on a Hewlett-Packard GeneArray Scanner. Results were analyzed with Affymetrix GeneChip Analysis Suite 4.0 (GAS) software. Individual microarrays were scaled to produce a mean signal intensity (average difference) of 2,500, excluding the top and bottom 2 percentile to remove outliers. The "average difference" describes the signal intensity difference between the match and mismatch probes for each gene averaged over the number of probe sets. Barring systematic error, the average difference reflects the amount of mRNA detected for each gene probed.

Clustering methods. We used three clustering methods to assess the relationship between expressed genes: hierarchical clustering, self-organizing maps, and anchor gene clustering. For hierarchical clustering, GAS software was used to calculate a "fold-change" value and to determine whether the change was statistically significant, i.e., increased, decreased, or unchanged. Microarrays from each time point were compared against three uninjured controls. This comparison of three replicates of each time point with three controls yields nine products, which we exported to Microsoft Excel spreadsheets for further analyses. To conservatively assess the reproducibility of the microarray hybridization results, we chose to average only the comparisons for which the GAS difference call was either "increased" or "decreased" in at least eight out of nine of the replicate comparisons. Fold-change values were calculated for these filtered results, which were then $\log_2$-transformed and subjected to hierarchical clustering using Cluster 1.1.1 and Treeview software for visualization (15).

For self-organizing maps, the average differences of three replicates for each time point were combined into a single mean only if they were in consensus on the GAS "present" call. Otherwise, the gene was assigned an artificial score of zero to denote absence of specific signal. We then filtered results using GeneCluster software (46) under default conditions (leaving 396 probe sets selected) and normalized to a mean of 0 and a variance of 1. The best fit to the smallest number of clusters was obtained by running 10,000 iterations of a 3 × 3 matrix of presumptive centroids. Several independent runs of the algorithm produced nearly identical clusters. Following clustering of the normalized data, the original average difference values for each gene were retrieved. The values for replicates were averaged, and these were substituted for the normalized values in the final display.

Anchor clustering used a Pearson product moment correlation coefficient to find temporal gene expression profiles that correlated with the profile of a selected "anchor" gene. Results were filtered for genes having at least one time point significantly different from uninjured controls as determined by ANOVA and the Duncan post-hoc test at the 95% confidence level.

Confirmation of RNA changes. We confirmed selected microarray results by comparison with mRNA levels obtained by quantitative reverse transcription PCR (Q-RT-PCR) using selected gene-specific primer pairs (Table 1) and cDNAs prepared from a separate time course study of rat SCI. Animals for the Q-RT-PCR time course were injured using the standard MASCIS protocol (see above) and were killed at 0 (intact controls), 12, or 24 h after injury (n = 3; one animal per RNA preparation). RNA was purified from a 5-mm segment of cord centered at the contusion site using the Trizol protocol and reverse transcribed with SuperScript II and random primers as suggested by the manufacturer. The PCR reactions were carried out using 10 ng of cDNA, 50 nM of each primer, and SYBR Green master mix (Applied Biosystems) in 20-μl reactions. Levels of Q-RT-PCR product were measured using SYBR Green fluorescence (40, 51) collected during real-time PCR on an Applied Biosystems model 7900HT system. A control cDNA dilution series was created for each gene to

[1]Supplementary Material to this article is available online at **http://physiolgenomics.physiology.org/cgi/content/full/7/2/201/DC1**.

Table 1. *Oligonucleotide primers used for Q-RT-PCR*

GenBank Accession No.	Name	Sequence
U88036	BDCP	5′-CGTCTTTACCTTGGATTGCCG-3′
		5′-GCTTCGTTTTCAGTCCTCCGTC-3′
AF058795	GABABR	5′-AGACTCTCTCCGTGACCTTGGG-3′
		5′-CTCTGACTGGGCTGTTCCTGTC-3′
X62840	KCP	5′-CCCCTGCTGTGACTGTATGCTC-3′
		5′-CGATGACTGACTGCCTTTTTGG-3′
U30938	MAP2	5′-CTGCGTTCCAGCGAGATGAC-3′
		5′-TGTGTGTGCGTGTGTGTGTGG-3′
M92076	MGLUR	5′-GACTGTTTCCCGCTTCTCTGG-3′
		5′-GCCATCGCCTGTCATCTGTG-3′
M28648	NALPH	5′-GCATCATCTCCGAGGGTAACG-3′
		5′-CATTCACACCATCGCCAGTCAC-3′
M25638	NF	5′-TCACCAGCGTGGGTAGCATAAC-3′
		5′-TTCTTCTCCTTCAGAGGGGGGC-3′
AF030253	VGAT	5′-TCGGCATCATCGTGTTCAGC-3′
		5′-AAGAAGGGCAACGGGTAGGAC-3′
AF106860	GAPDH	5′-AACTCCCTCAAGATTGTCAGCAA-3′
		5′-GGCTAAGCAGTTGGTGGTGC-3′
E13732	CCCR	5′-ACCTGTAGCCCTCATTTCCCC-3′
		5′-GCTGCTTGCTCTGCTCACACTG-3′
M19257	CRBP	5′-AGAAGGGAGAGAAGGAGGGACG-3′
		5′-CTGGGGTGGCTATGTGTTTCAG-3′
M19651	FRA	5′-ATCCCCGACCTCTGACCTATCC-3′
		5′-GCAGCCCCGATTTCTCATCC-3′
J02722	HemeOx	5′-TCTGGAGTCTTTGACCTGCTGC-3′
		5′-TCTGGGATTTTCCTCGGGG-3′
Z27118	HSP70	5′-CCTGAACAAGAGCATCAATCCG-3′
		5′-GAGTAGGTGGTGAAGGTCTGCG-3′
M26744	IL-6	5′-GCTCTGGTCTTCTGGAGTTCCG-3′
		5′-TGGATGGTCTTGGTCCTTAGCC-3′
AF013144	MAPK	5′-CCTTTGAGGGGGTAGCAGGAAC-3′
		5′-TGGGTTTGGGGGTGACTTATTG-3′

Q-RT-PCR, quantitative reverse transcription-polymerase chain reaction.

establish a standard curve. Each reaction was subjected to melting point analysis to confirm single amplified products.

RESULTS

To identify global patterns of mRNA expression after acute SCI, we collected tissue from rats injured with the highly reproducible MASCIS contusion model. The MASCIS model ensures delivery of a contusion with less than 5% deviation in height of weight drop, velocity of impact, and time of cord compression. Each rat received standardized doses of pentobarbital anesthesia and was injured 1 h after induction of anesthesia. After euthanasia, care was taken to prevent RNA degradation. Tissues were kept as cold as possible during dissection, and frozen samples were thawed in cold Trizol by homogenization.

We examined two segments of spinal cord: I, a 5-mm segment centered on the site of impact (at T9–10); and D1, a 5-mm distal segment adjacent to the impact segment. RNA changes in the I segment should reflect direct cellular damage and local responses, and changes in the D1 segment should reflect responses to diffusible signals and loss of synaptic input onto neurons residing in the D1 segment. We focused on the acute phase of injury, and on regions of spinal cord near the impact site to emphasize gene expression changes preceding secondary cell death. Cell death continues in the several days after this acute period, including apoptotic cell death (2). Methylprednisolone reduces cell loss in this time period (12).

To demonstrate the reproducibility of the MASCIS contusion model and to assess differences in cell survival between the I and D1 segments, we measured total tissue potassium in the Trizol homogenate. Cells that die lose their ionic gradients and release their potassium into extracellular fluid. Previous studies have shown that extracellular potassium diffuses from the injury site into the blood (12, 26). Therefore, tissue potassium content correlates linearly with cell volume fraction, the proportion of tissue that is comprised of potassium containing cells. Uninjured spinal cord tissues have a potassium concentration ($[K]_t$) of 92.0 ± 1.4 μmol K^+ per g tissue in the I segment. Figure 1 shows that this value fell to 42.6 ± 0.9 μmol/g by 6 h in the I segment and remained at approximately this level at 12, 24, and 48 h. However, the $[K]_t$ in the D1 segment declined more slowly, only reaching minimal values of 62.1 ± 1.8 μmol/g at 48 h. The standard deviations were less than 5% of the mean in I and D1 segments over all time points. The MASCIS contusion model results in a very reproducible injury. Cell loss was localized to the site of injury (I) at 6 h but spread over time into an adjacent, distal segment (D1).

We pooled RNA from 1–3 animals to obtain the 10 μg of total cellular RNA required for target preparation.

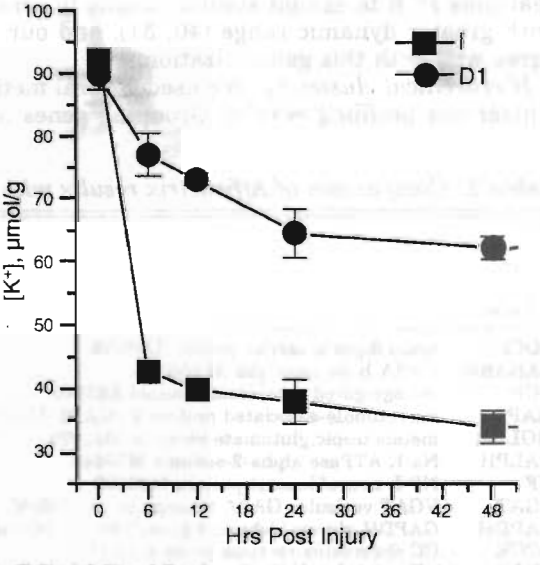

Fig. 1. Cell viability following contusion injury. Rats were injured using the MASCIS device by dropping a 10.0-g weight from a height of 25.0 mm onto exposed T9–10 spinal cord. At 6, 12, 24, and 48 h after contusion, animals were killed, their spinal cords were quickly removed to ice, and the cords were sectioned on dry ice into 5-mm segments, then weighed. The I segment encompassed the contusion site, and the D1 segment was immediately distal (caudal) to the I segment. Frozen tissues were homogenized in Trizol, and an aliquot was removed, diluted in water, and sonicated, then analyzed for total tissue K by atomic absorption spectroscopy. Tissue potassium concentration, $[K^+]$, was expressed as micromoles of potassium per gram wet weight of tissue. Results were obtained from a separate time course study of injury with 4 animals (2 male and 2 female) injured at each time point. Values are means ± SE.

Such pooling was necessary due to variability of RNA extraction and RNA loss in injured spinal cords. Microarray results were quite reproducible, however. All background and noise (the RawQ parameter from the Affymetrix GAS software) measurements were well within limits considered acceptable by Affymetrix. Average differences that were judged to be "present" in all replicates by GAS software were compared by linear regression. Correlation coefficients calculated between each pair of replicates were greater than 0.77 (r^2 value). Finally, we compared the mean of the average difference for selected genes over three replicates with gene expression levels measured by Q-RT-PCR. Table 2 shows a comparison of the two different measures. RNA measurements are expressed as fold changes with respect to RNA levels in uninjured tissues, and the variance is the standard error of the mean. Affymetrix results are marked with an asterisk (consistently different mRNA levels from uninjured controls) based on the criteria used for hierarchical clustering (see below). For each of the genes measured by Q-RT-PCR, the mRNA levels were shown to change in the same direction as the changes measured by microarray detection. All time points assayed by Q-RT-PCR were found to differ significantly from controls by Q-RT-PCR (as determined by Student's t-test at $P < 0.05$), except glyceraldehyde-3-phosphate dehydrogenase (GAPDH) levels, which were found to be unchanged in agreement with Affymetrix results. Previous studies have shown real-time PCR to exhibit similar results to arrays (38) with greater dynamic range (40, 51), and our results agree well with this generalization.

Hierarchical clustering. We used several methods to cluster our profiling results. Grouping genes by their observed temporal profiles should cluster genes with similar patterns of regulation or similar responses to signaling mechanisms. For hierarchical clustering, fold-change results were filtered to a high stringency. First, each replicate time point ($n = 3$) was compared with an uninjured control ($n = 3$), since there was no a priori reason to pair any one experimental result with any one control. From these nine comparisons, we selected only genes with a GAS difference call (increased, decreased, or no change from control) that matched in at least eight of nine cases and calculated the mean fold-change value. In cases where GAS judged the control (denominator) average difference value to be below the threshold of significance, GAS calculated a minimum fold-change value using the threshold, and this value was used here. All other comparisons were marked with a fold-change value of 1, indicating no significant change. This dataset was $\log_2$-transformed, imported into Cluster 1.1.1 software (15), and then filtered for probes having at least one observation with a mean fold change of 4 ($\log_2$ of 2). In the I segment, only 137 probes remained after this filtering. Data were then normalized and sorted by complete linkage clustering using the uncentered correlation similarity metric. The resulting dendrogram depicts the mRNAs that differ from control by at least a factor of four at one time point or more (Fig. 2, *left*). The identity of the genes and their associated fold changes are presented in Table 3. The number of genes that changed expression levels at 6 h was greater than at 12 h. However, the number of genes that changed increased at 24 and 48 h.

In the I segment dendrogram, we found clusters of genes with similar biological function. One cluster con-

Table 2. *Comparison of Affymetrix results with Q-RT-PCR*

		Fold Change			
		Affymetrix		Q-RT-PCR	
Name	Description	12 h	24 h	12 h	24 h
BDCP	brain digoxin carrier protein U88036	−12.4 ± 4.4*	−12.8 ± 3.8*	−5.11 ± 0.47†	−4.10 ± 0.35†
GABABR	GABA-B receptor gb2 AF058795	−3.6 ± 1.7	−7.0 ± 2.2*	−4.92 ± 0.56†	−4.92 ± 1.16†
KCP	voltage-gated potassium channel X62840	−6.3 ± 3.3	−8.9 ± 1.5*	−65.4 ± 8.44†	−74.1 ± 38.2†
MAP2	microtubule-associated protein 2 (MAP2) U30938	−17.4 ± 13.0*	−21.8 ± 16.2*	−19.6 ± 2.48†	−39.8 ± 14.0†
MGLUR	metabotropic glutamate receptor M92076	−8.6 ± 3.1*	−14.0 ± 2.7*	−1.69 ± 0.42†	−1.98 ± 0.03†
NALPH	Na-K-ATPase alpha-2-subunit M28648	−9.4 ± 6.7	−12.6 ± 2.5*	−6.73 ± 1.01†	−4.11 ± 1.49†
NF	NF-L neurofilament protein M25638	−52.7 ± 26.9	−42.0 ± 9.5*	−5.97 ± 0.60†	−3.14 ± 0.10†
VGAT	VGAT vesicular GABA transporter AF030253	−17.6 ± 8.0	−19.8 ± 4.8*	−91.5 ± 24.8†	−64.2 ± 41.1†
GAPDH	GAPDH glyceraldehyde-3-phosphate dehydrogenase X02231	1.0 ± 0.4	1.2 ± 0.8	0.97 ± 0.04	1.26 ± 0.17
CCCR	CC chemokine receptor protein E13732	10.0 ± 5.1	8.4 ± 2.1*	19.1 ± 3.44†	15.3 ± 0.72†
CRBP	cytosolic retinol-binding protein (CRBP) M19257	4.0 ± 3.8	15.0 ± 5.4*	1.97 ± 0.036†	3.73 ± 0.13†
FRA	Fra-1; fos-related antigen; proto-oncogene M19651	15.7 ± 6.6	8.2 ± 1.7*	118 ± 20.6†	66.5 ± 2.19†
HemeOx	heme oxygenase J02722	42.7 ± 18.3	89.3 ± 20.3	9.16 ± 0.60†	10.4 ± 0.62†
HSP70	heat shock protein 70 (HSP70) EST AA848563	22.4 ± 14.6	16.2 ± 7.5*	3.78 ± 0.33†	3.56 ± 0.42†
IL-6	IL6 interleukin 6 M26744	47.4 ± 40.5	6.4 ± 2.2	85.5 ± 19.7†	18.6 ± 2.31†
MAPK	cpg21 MAP-kinase phosphatase AF013144	15.6 ± 7.7	10.2 ± 1.1*	15.4 ± 2.46†	9.42 ± 0.57†

Affymetrix results are expressed as fold change from uninjured control mRNA levels ± SE; $n = 3$. Measurements of RNA with Q-RT-PCR were obtained from a separate group of animals than the Affymetrix study. Reactions were run on an Applied Biosystems model 7900HT sequence detection system, using the SYBR Green protocol. A dilution series of control cDNA served as a standard curve, producing values for each time point that represent fold change of control. All results were within the standard curve range, and all PCR reactions exhibited single melting point peaks, indicating a single amplified product. *Results with greater than 80% (≥8/9) consensus of either "Increased" or "Decreased" call by Affymetrix GAS algorithms. †Results of Q-RT-PCR that are significantly different from uninjured, control spinal cord by Student's t-test at $P < 0.05$.

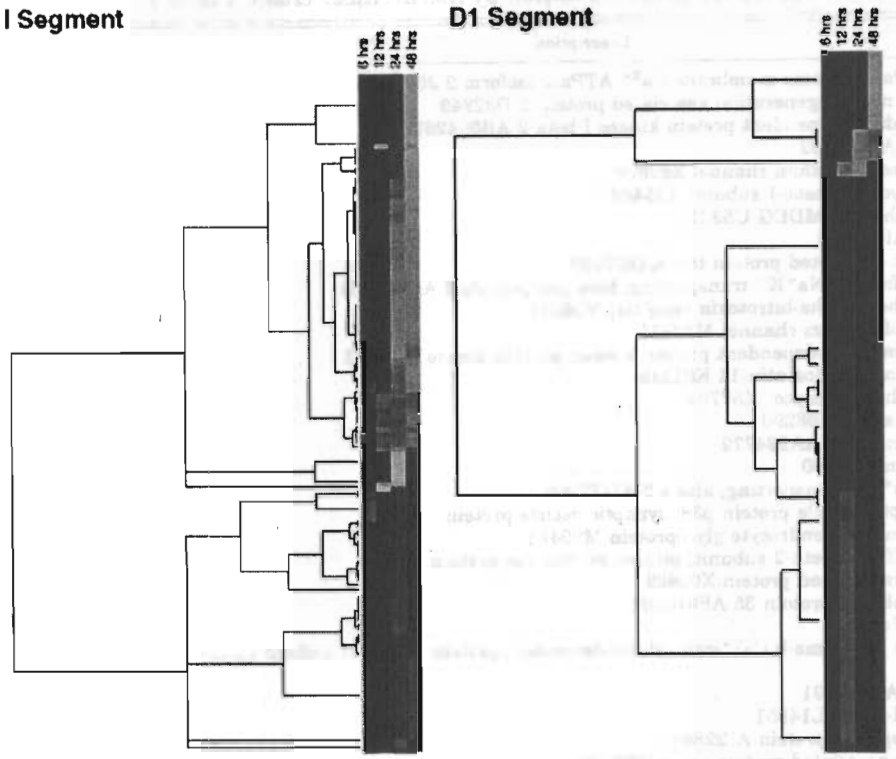

Fig. 2. Hierarchical clustering of Affymetrix fold-change results from I segment (*left*) and D1 segment (*right*). The fold-change data (compared with uninjured control spinal cord) was filtered to select only changes with highly reproducible "difference calls." The Affymetrix Gene Analysis Suite algorithm judges a fold change to be an increase or a decrease only if several thresholds are met. We chose to perform comparisons between all three replicates at each time point against all three control replicates, yielding nine comparisons, and then to average only those comparisons where at least 80% of the difference calls were unanimous (either increase or decrease). Comparisons that failed this test were assigned a fold change of 1. Data were $\log_2$-transformed, normalized, and clustered as described in the text. Green represents a decreased fold change, and red represents increased fold change. Brighter colors represent greater fold changes. Black indicates no change, or inconsistent results. Columns represent time after injury compared with uninjured control spinal cord, and rows represent individual gene probes. Results from the I segment dendrogram are expanded in Table 3; D segment dendrogram results are expanded in Table 4. Results for all genes probed may be found in the form of a searchable database at **http://spine.rutgers.edu/microarray**.

tains genes that are increased at 6 h, and this group includes many inflammatory cytokines [interleukin-1β (IL-1β), IL-6, macrophage inflammatory protein-1α (MIP-1α), and MIP-2]. A second cluster near the top of the dendrogram represents mRNAs that diminished over the 48 h following injury. Many of these genes are associated with neuronal function (e.g., SNAP-25A, citron, synapsin II, tau, vesicular GABA transporter, sodium-dependent neurotransmitter transporter). We interpret the pattern and composition of this cluster as being consistent with selective and progressive loss of neurons.

Gene expression results for the D1 segment were clustered using identical methods (Fig. 2, *right* and Table 4). We hypothesized that the less injured distal segment should have fewer responding mRNAs and that response to injury may be delayed or diminished. Indeed, the D1 fold-change results showed many fewer changes and a delayed response to contusion. This stringent analysis revealed only eight mRNAs that declined, probably reflecting the relative lack of cell-type-specific loss in D1 during the first 48 h after injury compared with I. Few mRNAs differed from control at the 6-h time point. However, many genes that have increased expression at 6 h in the I segment can be seen to increase in the D1 segment at 12 h.

Self-organizing maps. We used a second clustering method to distinguish temporal patterns. A self-organizing map plots mRNA levels over n time measurements from each gene as a single point in n-dimensional space. Randomly placed nodes are added and iteratively moved closer to clusters of microarray data by applying a distance formula and moving nodes toward adjacent data points. By minimizing the distance of the nodes to nearby data points, the nodes come to represent the centroid of a cluster of nearby data points. The number of centroids created for this process is determined by the user. After several trials, we settled on a 3×3 matrix of centroids as our starting point, since this gave the best balance of fit to the data

Table 3. *Fold-change values for genes identified by hierarchical clustering of I segment*

ID	Description	6 h	12 h	24 h	48 h
1	PMCA ATPase; plasma membrane Ca^{2+} ATPase-isoform 2 J03754	−3.9	−5.6	−6.6	−9.2*
2	Neurodap1 neurodegeneration associated protein 1 D32249	−1.9	−4.1	−6.7	−5.5*
3	Ca^{2+}/calmodulin-dependent protein kinase I beta 2 AB004267	−2.8	−2.6	−6.3	−8.5*
4	SNAP-25B AB003992	−3	−20.3	−16.3	−31.5*
5	voltage-gated potassium channel X62839	−1.8	−4.2	−3.6	−5.7*
6	GABA(A) receptor beta-1 subunit X15466	−2.3	−6.9	−7.5	−9.3*
7	degenerin channel MDEG U53211	−2.2	−1.8	−2.5	−5*
8	lipophilin AI072770	1.3	0.1	−1.3	−4*
9	microtubule-associated protein tau AA957930	−1.4	−2.1	−3.5	−4.3*
10	ATPase isoform 2, Na^+K^+ transporting, beta polypeptide 2 AA943784	−3.9	−4.5	−4.2	−5.5*
11	neurexin I-beta alpha-latrotoxin receptor; M96375	−1.7	−9.1	−7.7	−8.7*
12	Na^+ channel; sodium channel M22254	−3	−4.2	−4	−5.1*
13	calcium/calmodulin-dependent protein kinase; protein kinase M16112	−2	−3.1	−5.5	−7.5*
14	somatostatin; somatostatin-14 K02248	−1.7	−2.2	−2.5	−5*
15	ET-B endothelin receptor X57764	−0.8	−5.3*	−4.9	−6.9*
16	neuronatin alpha U08290	−1.2	−1.8	−2.3*	−4.7*
17	metallothionein-III AA924772	−1.5	−1.8	−2.2*	−4.7*
18	somatostatin M25890	−2.1	−4.2	−3.8*	−14.7*
19	ATPase, Na^+K^+ transporting, alpha 2 AI177026	−1.3	−2.1	−2.9*	−12.6*
20	major synaptic vesicle protein p38; synaptic vesicle protein X06655	−2.7	−3.4*	−4.3*	−13.7*
21	MOG myelin/oligodendrocyte glycoprotein M99485	−0.1	−1.9*	−2.6*	−6.1*
22	(Na^+,K^+)-ATPase-beta-2 subunit; plasma membrane protein J04629	−0.8	−0	−2.6*	−4.1*
23	rab3 gene; ras-related protein X06889	−3.8	−4.5	−6.8*	−15.5*
24	neural membrane protein 35 AF044201	−1.4	−0.9	−2.9*	−4.6*
25	zyginI U63740	0	−1.5	−2.8*	−5.3*
26	CaM kinase II gamma-b Ca^{2+}/calmodulin-dependent protein kinase II isoform gamma-b S71570	−2	−3.4	−6.9*	−11.3*
27	SNAP-25A AB003991	−2.5	−10.5	−8.5*	−9.5*
28	neurexin III-alpha L14851	−3.7	−7.8	−8.7*	−13.4*
29	GABA transporter protein AI228669	−1.5	−3.4	−5.6*	−10.2*
30	microtubule-associated protein tau AI227608	−1.2	−2	−3.6*	−5.6*
31	microtubule-associated protein 2 X53455	−2.7	−7.3	−6.6*	−8.9*
32	sodium-dependent neurotransmitter transporter S56141	−2.7	−4.3	−5.8*	−7.8*
33	RK5 K^+ channel protein; M59980	−3.2	−6.4	−5*	−6.4*
34	protein kinase C type III K03486	−4.2	−5.4	−4.8*	−6.4*
35	voltage-gated potassium channel X62840	−4.6	−6.3	−8.8*	−12.3*
36	synapsin II AI145494	−2.6	−4.1	−5.1*	−6
37	NP25 neuronal protein M84725	−1.6	−1.8	−4.7*	−6.3*
38	neurotrimin U16845	−2.3	−8.3	−9.3*	−11.3*
39	Na,K-ATPase Na,K-ATPase alpha-2-subunit M28648	−5.9	−9.4	−12.6*	−16.3*
40	GABA-B receptor gb2 AF058795	−2.9	−3.6	−7*	−8.4*
41	VGAT vesicular GABA transporter AF030253	−13.8	−17.6	−19.8*	−25.8*
42	trkB neural receptor protein-tyrosine kinase M55291	−3.2	−10.8	−11.5*	−15*
43	putative four repeat ion channel AF078779	−2.9	−3.9	−4.5*	−5.6*
44	limbic system-associated membrane protein U31554	−5.1	−9.2	−7.6*	−9.6*
45	NPH-type III PD-Ialpha; nucleotide pyrophosphatase; phosphodiesterase I D28560	0.4	−3.1	−11.6*	−8.7*
46	putative four repeat ion channel AF078779	−2.9	−3.9	−4.5*	−5.6*
47	potassium channel protein; transmembrane protein X12589	−1.6	−15.9	−17.8*	−20.7*
48	Mtap-1 microtubule-associated protein 1A M83196	−1.4	−2.6	−3.8*	−4.1*
49	potassium channel potassium channel protein M26161	−2.4	−7.4	−10*	−10.4*
50	postsynaptic density protein (citron) AI059948	−2.5	−3.2	−3.9*	−4.2*
51	SNAP-25A AB003991	−2.5	−10.5	−8.5*	−9.5*
52	heavy neurofilament polypeptide NF-H X13804	−8.9	−15.8	−17.6*	−21.9*
53	brain acyl-CoA synthtase II D30666	−1.3	−3.9	−9.2*	−7.7*
54	BFP brain finger protein AF054586	−3.9	−9.8	−11.2*	−8.9*
55	NPH-type III PD-Ialpha; nucleotide pyrophosphatase; phosphodiesterase I D28560	0.7	−3.4	−9.6*	−10.1*
56	CCHL2A dihydropyridine-sensitive L-type calcium channel alpha-2 subunit M86621	−2	−2.9	−6.5*	−4.6*
57	C1C-3 protein kinase C-regulated chloride channel D17521	−1.3	−5.6	−6*	−4.3*
58	ATPase Na^+/K^+ transporting beta 1 AI112173	−1.8*	−3.3	−4.1*	−4.7*
59	NF-L neurofilament protein M25638	−7.6*	−52.7	−41.9*	−83.8*
60	neurofilament protein Z12152	−3.8*	−10.1	−13.5*	−27.1*
61	light molecular-weight neurofilament (NF-L) AF031880	−3.9*	−8.6	−10.3*	−24*
62	neurofilament, heavy AA818677	−4.4*	−8.8	−9.3*	−20*
63	EST AI102079	−2.8*	−3	−4.5*	−5.7*
64	syntaxin B M95735	−2.8*	−2.9	−3.7*	−5.4*
65	microtubule-associated protein 2 (MAP2) U30938	−2.7*	−17.4*	−21.8*	−21.7*
66	MAP2C; microtubule-associated protein X17682	−4.3*	−9.7*	−8*	−10.6*
67	Na^+ channel; sodium channel M22253	−7.1*	−14.1*	−16.1*	−23.2*
68	PEP-19 neuron-specific protein M24852	−3.7*	−5.9*	−8.7*	−11.4*
69	ATPase Na^+/K^+ transporting beta 1 AI230614	−2.7*	−7.1*	−7.7*	−12.2*

Continued

Table 3. *Continued*

ID	Description	6 h	12 h	24 h	48 h
70	neurodegeneration associated protein 1 AA894089	−2.4*	−4.3*	−4.7*	−8.8*
71	GS-alpha subunit; GTP-binding protein alpha subunit; alternative splicing L10326	−2.5*	−3.9*	−5*	−8.1*
72	brain digoxin carrier protein U88036	−5.3	−12.3*	−12.8*	−13.9*
73	G-alpha-0 GTP-binding protein M17527	−1.9	−4.3*	−4.9*	−8.3*
74	protein kinase C X04139	−2.8	−6.1*	−7.6*	−10.2*
75	glutamate receptor; metabotropic glutamate receptor M92076	−1.7	−8.5*	−13.9*	−17.4*
76	calcineurin A alpha; calmodulin-dependent protein phosphatase; isoform D90035	−1.8	−9.7*	−20.1*	−9.8*
77	tau microtubule-associated protein X79321	−1.3	−2.5	−4.2*	−6.2
78	Shal1 K^+ channel S64320	−2.2	−4.1	−6.1*	−5.3
79	synapsin II AI145494	−3.3	−6.3	−7.9*	−11.4*
80	synapsin 2a synapsin 2a M27925	−3.3	−3.8	−5.8*	−6.9
81	chemokine CX3C AF030358	−1.2	−2.3	−4.9*	−2
82	NCKX2 potassium-dependent sodium-calcium exchanger AF021923	−1.6	−4.9	−5.4*	−6.4
83	insulin-like growth factor M15481	−1	−6.9*	−8.1*	0.1
84	heat shock related protein AI171166	−2	−4.3*	−4.9	−4.4
85	macrophage inflammatory protein-2 precursor U45965	23.4*	28.9	11.7*	2.7
86	cpg21 MAP-kinase phosphatase AF013144	14.2*	15.6	10.1*	4.8
87	interleukin 6 M26745	19.4*	16.8	1.8	1.6
88	IL6 interleukin 6 M26744	61.9*	47.3	6.4	2.8
89	macrophage inflammatory protein-1alpha U22414	17.8*	23.2	9.5	4.4
90	interleukin 1-beta M98820	14.1*	15.4	5.1	1.3
91	heme oxygenase AI179610	6.4*	15.7*	36.6*	28*
92	heme oxygenase J02722	14.4*	42.6*	89.3*	88.7*
93	metallothionein AI176456	4.4*	4.5*	3.9*	2.8*
94	metallothionein AI102562	8.6*	5.9*	5.5*	5.2*
95	rNFIL-6 C/EBP-related transcription factor S77528	6.1*	11.9*	10.3*	11.2*
96	sfb silencer factor B X60769	6.3*	9.4*	8.3*	5.6*
97	JE immediate-early serum-responsive gene (MCP-1) X17054	39.1*	39.6*	46.1*	35.8*
98	JE immediate-early serum-responsive gene (MCP-1) X17053	28.2*	31.1*	36.8*	21.6*
99	hsp70.2 heat shock protein 70; Z75029	4.8*	5.5	5.9*	3.2*
100	heat shock protein 70; hsp70 gene Z27118	10.8*	20.7	14.5*	7.2*
101	hsp70.2 heat shock protein 70 AI071965	6*	7.9	5.9*	3.7*
102	HSP70 heat shock protein 70 L16764	9.3*	9.4	7.9*	4.3*
103	Fra-1; fos-related antigen; proto-oncogene M19651	11.2*	15.6	8.1*	6.6*
104	heat shock protein 27 (hsp 27) AA998683	2.3*	2.6	3.9*	4.3*
105	metallothionein-1 and -2 M11794	9.2*	7.7*	6.8	6.2*
106	VGF nerve growth factor; secretory protein M74223	1.8	8.2	8.9*	8.4*
107	nestin M34384	3.6	5.1	11.2*	10.8*
108	vimentin X62952	1.4	2.2	5.8*	6.8*
109	ESTs, highly similar to integrase interactor 1a protein AI171319	−0.4	2.5	4.7*	4.8*
110	peripheral-type benzodiazepine receptor J05122	2.5	8.2	14.3*	16.2*
111	CC chemokine receptor protein E13732	4.1	9.9	8.3*	6.3*
112	heat shock protein 70 (HSP70) AA818604	5.2	7	8*	3.7*
113	galanin J03624	2.3	4.3	6.9*	4.4*
114	TGF-beta 1; transforming growth factor-beta 1 X52498	4.5	8.1	11.2*	29.1*
115	protein kinase C receptor U03390	−0.4	1.1	3.4*	4.4*
116	cytosolic retinol-binding protein (CRBP) M19257	0	4	14.9*	26.1*
117	40-kDa ribosomal protein D25224	0.7	1.6	3.5*	4.4*
118	catechol-O-methyltransferase M93257	0.1	1.6	3.1*	7.2*
119	beta-integrin S44606	0.5	1.9	2.7	4.8*
120	glia-derived neurite-promoting factor (GdNPF) AI229707	−2.2	0.2	3.2	8.4*
121	ESTs, moderately similar to synaptogyrin AA799879	−0	1.3	2.5	4.9*
122	HSP27 heat shock protein 27 M86389	2.5	3.4	5.2	7.3*
123	TNF receptor tumor necrosis factor receptor M63122	4.3	7.2	8.4	12.4*
124	catechol-O-methyltransferase M60753	−0.2	3	6.2	15.9*
125	P-selectin L23088	4.1	3.3	2.4	4.4*
126	GLUT1 transporter C-terminal binding protein AF032120	−0.6	0.3	2.7	5.7*
127	interleukin 4 receptor X69903	2.9	3.9	3.3	4.8*
128	oncoprotein p53 X13058	−0.4	1.3	3.2	4.2*
129	CXCR4 CXC chemokine receptor U90610	−0.1	1.6	2.5	5*
130	CXCR4 CXC chemokine receptor U90610	−0.1	1.6	2.5	5*
131	rBax alpha U49729	−0.7	2.1	4.2	4.7*
132	P2x4 ATP Receptor U47031	0.2	1.6	3.4	5*
133	BDNF = brain-derived neurotrophic factor S76758	1.6	3.1	3.8	5.7*
134	bax apoptosis inducer S76511	0.9	2.8	4.6	5*
135	iNOS nitric oxide synthase U03699	4.9	14.3	5.6*	2.4
136	heat shock protein 70 (HSP70) EST AA848563	9.5	22.3	16.2*	7.8
137	intercellular adhesion molecule-1; ICAM-1 D00913	6.9	4.1*	3.2	2.8

*Results with greater than 80% (≥8/9) consensus of either "Increased" or "Decreased" call by Affymetrix GAS algorithms.

Table 4. *Fold-change values for genes identified by hierarchical clustering of D1 segment*

ID	Description	6 h	12 h	24 h	48 h
1	microtubule-associated protein tau AI227608	−0	−3.3	−3.1	−4.3*
2	ATPase, Na^+K^+ transporting, alpha 2 AI177026	0.3	−1.5	−1.4	−4*
3	Na^+ channel; sodium channel M22253	0.2	−4.5	−0.6	−4.1*
4	GABA-B receptor gb2 AF058795	−0	−5.1	−1	−4.2*
5	NGFI-B U17254	−2.9	−2.7	−8.4	−6.2*
6	IGFII insulin-like growth factor X17012	−3.4	−1.2	−9.3*	−6.1*
7	NGFI-A AF023087	−1.1	0.8	−5.5*	−4.6*
8	insulin-like growth factor M15481	−2.9	−6*	−10*	−1.5
9	TGF-beta 1; transforming growth factor-beta 1 X52498	0.8	5	1.9	10.8*
10	ESTs, Highly similar to integrase interactor 1a protein AI171319	5.9	7.7	7.5	13*
11	neurocan M97161	−1.2	3.7	5	9.7*
12	VGF nerve growth factor; secretory protein M74223	1.4	2.7	1.4	4*
13	cytosolic retinol-binding protein (CRBP) M19257	−0.7	2.1	1	8.6*
14	peripheral-type benzodiazepine receptor J05122	1.4	4.3	3.4	13.3*
15	beta-actin V01217	1.2	3.4	3.2	4.4*
16	beta-actin V01217	1.1	4.9	4.2	7.9*
17	GFAP delta alt spliced AF028784	−0	4.6	5.8	10.6*
18	class I beta-tubulin AB011679	0.1	1.5	1.9	4.7*
19	vimentin X62952	0.3	1.9	1.7	5.6*
20	JE immediate-early serum-responsive gene (MCP-1) X17053	4.1*	23*	1.6	8.1*
21	metallothionein AI102562	8.6*	6.8*	2.8	7.7*
22	metallothionein AI176456	3.7*	4.1*	3.1*	4.6*
23	metallothionein-1 and -2 M11794	10.9*	10.4*	5.8*	10*
24	heme oxygenase AI179610	3.6*	19.7*	6.4*	34.7*
25	heme oxygenase J02722	4.1	38.9*	11.4*	70*
26	HSP27 heat shock protein 27 M86389	6.6	19.5*	23.1*	32.6*
27	heat shock protein 27 (hsp 27) AI176658	0.6	3.6*	3.8*	4.7*
28	heat shock protein 27 (hsp 27) AA998683	0.8	4.3*	4.3*	5.7*
29	sfb silencer factor B X60769	2.3	9.7*	2	3.5*
30	JE immediate-early serum-responsive gene (MCP-1) X17054	9.8	39.1*	2	15.3*
31	MnSod gene; superoxide dismutase Y00497	1.6	4.5*	2.1*	1.3
32	SOCS-3 suppressor of cytokine signaling-3 AF075383	2.2	9.2*	2.6	4.4
33	cpg21 MAP-kinase phosphatase AF013144	2.3	8.3*	1.9	1.1
34	interleukin 4 receptor X69903	2.4	5.1*	2.2	4.2
35	macrophage inflammatory protein-2 precursor U45965	1.7	26.4*	−0.3	−0.8
36	rNFIL-6 C/EBP-related transcription factor S77528	2.9	9*	2.5	3
37	FGFR-1 beta fibroblast growth factor receptor 1 beta-isoform S54008	3.7	6.3*	3.2	3.9
38	interleukin 6 M26745	3.8	23.8*	−1.5	0.7
39	PDE4 phosphodiesterase M25350	1.2	4.4*	1.7	1.2
40	Fra-1; fos-related antigen; proto-oncogene M19651	4.9	15.6*	0.7	1.2
41	HSP70 heat shock protein 70 L16764	0.6	12.2*	0.5	2.8
42	cAMP phosphodiesterase J04563	4.5	5.4*	0.9	−0.4
43	CC chemokine receptor protein E13732	−0.8	5.1*	1.3	2.4
44	FGF receptor-1; fibroblast growth factor receptor D12498	0.6	5*	2.9	3.6
45	IL6 interleukin 6 M26744	8.6*	63.8*	0.9	1.8

*Results with greater than 80% (≥8/9) consensus of either "Increased" or "Decreased" call by Affymetrix GAS algorithms.

with the number of centroids. Following a typical 10,000 iterated run of the GeneCluster software (46), clusters were output to Excel, where the means and standard deviations of the filtered average difference values were calculated and are displayed in Fig. 3.

This method proved to be useful for visualizing natural temporal patterns in our dataset. Two patterns paralleled those found by hierarchical clustering. First, *cluster 0* consisted of mRNAs that were relatively more abundant at 6 h and diminished thereafter. This group included the major inflammatory cytokines IL-1β, IL-6, MIP-1α, and MIP-2. Several of these had previously been identified as peaking at ~6 h after injury (1, 21, 45). Similarly, *clusters 3* and *6* reflected the neuronal loss that we had observed by hierarchical clustering, but included more species of mRNA. Additional clusters exhibited characteristic temporal patterns, with some diminishing and some increasing (*clusters 2*, *5*, and *8*) over the 48-h period. Although there are many genes in these clusters that are likely important in SCI biology, we were unable to find groups of genes that paired so well with the hierarchical clustering data or that matched so well by function as the neuronal and inflammatory groups.

Anchor clustering. We used a third clustering method to identify genes with a temporal expression pattern that mirrors one or more injury processes. After choosing "anchor" genes we can identify other genes that show a similar temporal pattern and, therefore, may be involved in a similar biological process. Figure 4 shows four sample anchor clusters: those for phosphodiesterase 4 (PDE4), neurofilament, nestin, and glia-derived neurite promoting factor (GdNPF). Three of the genes (PDE4, neurofilament, and nestin) are known to be involved in CNS injury or repair, but they have not been studied directly in SCI. GdNPF was

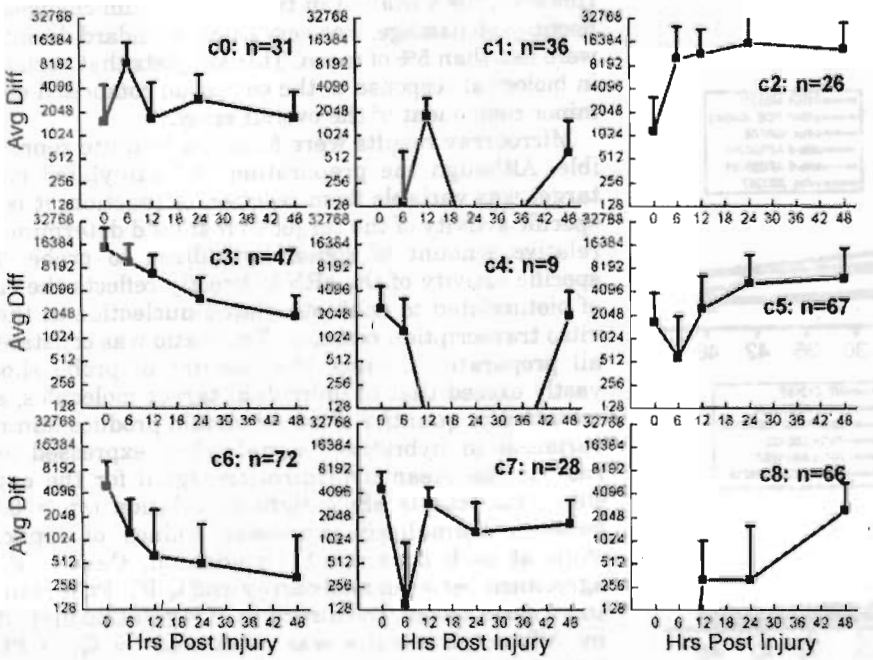

Fig. 3. Self-organizing map analysis of Affymetrix average difference results from the I segment. Average difference values were averaged only if the absent/present calls of all three replicates were in consensus, or else a value of 0 was assigned. The filtered data set was then $\log_2$-transformed, filtered, and clustered as described in the text. The mean, filtered average difference values (the centroids) of the identified clusters identified were then plotted on a $\log_2$ scale, with the standard error of the mean indicated in the positive direction. Identities of all clustered genes may be found in the form of a searchable database at **http://spine.rutgers.edu/microarray**.

chosen as a novel target for study. In each case we show the five closest correlates for each anchor gene, using the Pearson product moment correlation coefficient as the metric. After experimenting with different measures of similarity, we chose a correlation method because of the ability to find meaningful biological relations as measured by previously reported relationships. We screened results with ANOVA, using the Duncan post-hoc test at the 95% confidence level, to identify genes that differed significantly from control.

Functional group clustering. Finally, we examined genes representing specific biological pathways of interest. Figure 5*A* depicts patterns of selected stress responses in I and D1 segments. Figure 5*A*, *top*, shows four inflammatory cytokines or chemokines, the *middle* shows three stress-regulated transcription factors, and the *bottom* contains three likely responses to inflammatory or stress signaling. These results support our hypothesis that the inflammatory and stress responses are delayed in the D1 segment compared with the I. Cytokine mRNAs peaked at 6 h in the I segment but were delayed to 12 h in the D1. Similarly, c-fos, NFκB p105, and NGFI-A all followed the same pattern. Selected stress and inflammatory transcriptional regulators, Hsp70, ICAM-1, and SOCS-3, follow the same general pattern, peaking at 6 h in I and 12 h in D1, but they exhibit a more prolonged increase, particularly in the I segment.

Since GAP-43 is highly associated with neurite outgrowth, we compared its profile with those of two neurofilament transcripts, used here as markers of postmitotic neurons (Fig. 5*B*). In contrast to the general diminution of neuron-specific mRNA levels, GAP-43 increases slightly in the I segment and more robustly in the D1 segment. If GAP-43 expression is truly neuronal, then this may indicate that neurons distal to the injury are increasing neurite outgrowth during the acute phase of injury. More importantly, it suggests that neurons spared within the I segment are likely responding to injury by upregulating GAP-43. These predictions must be confirmed by in situ hybridization to localize gene expression and by functional assays to demonstrate growth.

DISCUSSION

To demonstrate the usefulness of microarrays for measuring changes in gene expression after SCI, several issues must be addressed. One concern is the variability inherent in biological systems, and particularly in injury models. We selected the MASCIS model of rat SCI because it causes spinal cord lesions that resemble human injury (35) and because of the reproducible nature of the model (e.g., see Fig. 1). The MASCIS protocol minimizes biological variability with its rigorous control of anesthesia, impact parameters, and postsurgical care. The MASCIS model also shows little variability in injury severity between males and females. Analysis of the over 6,000 animals injured under the strict criteria of the MASCIS model show no overall differences in lesion volume or functional deficits between the two sexes (Erkan K, Sun D, Hart RP, and Young W, unpublished results). However, the preliminary results of an ongoing study in our laboratory show a difference in the lesion volumes of female rats injured at various times during the estrus cycle. We are currently identifying cycle-dependent mRNA changes using microarrays. Because our groups were heterogeneous with respect to sex and the females were not screened for estrous stage, sex and estrous cycle differences may have contributed to overall variability.

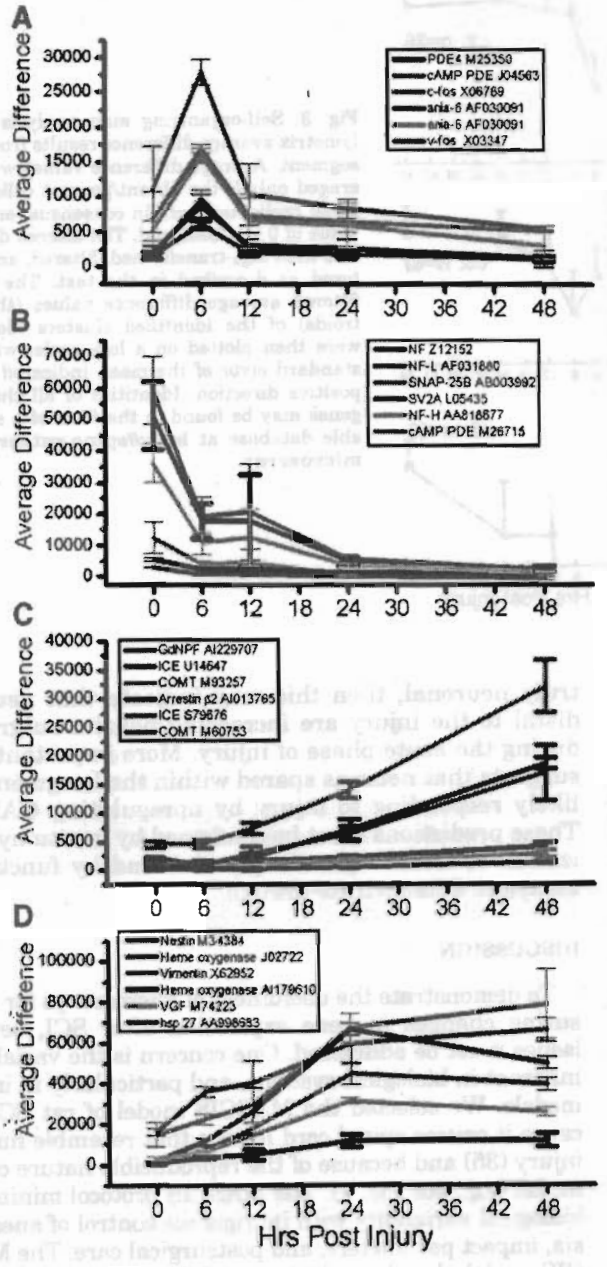

Fig. 4. Anchor clustering using genes of interest: phosphodiesterase 4 (*A*), neurofilament (*B*), glia-derived neurite promoting factor (GdNPF; *C*), and nestin (*D*). The temporal pattern of a gene of interest was used as a template for clustering under the assumption that genes which correlate highly are more likely than randomly matched ones to be regulated similarly or to share similar function. The Pearson product moment correlation coefficient was used to find the five genes whose temporal profile most closely resembles the anchor gene (listed at the *top* of each *inset* and marked with a black line). All profiles shown have at least one time point that differed from control by ANOVA and the Duncan post-hoc test at 95% confidence levels. The *y*-axes scales differ and are adjusted to facilitate identification of transcripts whose patterns overlap.

However, the variation in tissue potassium changes, reflecting cell damage, was very small; standard deviations were less than 5% of mean. This suggests that variations in biological response to the contusion comprised only a minor component of the overall error.

Microarray results were found to be quite reproducible. Although the preparation of biotinylated cRNA target was variable from reaction to reaction, it is the specific activity of the target that should determine the relative amount of signal hybridized to probe. The specific activity of the cRNA directly reflects the ratio of biotinylated to nonbiotinylated nucleotide in the in vitro transcription reaction. This ratio was constant in all preparations. Since the amount of probe should vastly exceed that of individual target molecules, any variation in quantity of target should produce minimal variation in hybridized signal when expressed as a ratio to the mean hybridization signal for the entire chip. Our results show tight correlation ($r^2 > 0.77$) between normalized expression values of replicate chips at each time point. In addition, there is close agreement between microarray and Q-RT-PCR results. In all cases tested, the direction of regulation predicted by Affymetrix results was confirmed by Q-RT-PCR. Variation between these methods in measuring regulation could be explained by a larger variability in some Affymetrix results or by inaccuracies in measuring lower concentrations of mRNA on microarrays (not shown). Others have found good agreement between Q-RT-PCR and microarrays when measuring higher concentrations of mRNA (38). Overall, microarray results were found to be reproducible.

The most striking pattern in our results was the spreading wave of inflammatory activity and stress responses following contusive SCI. Figure 5*A* shows IL-1β, IL-6, and MIP-1α increased at 6 h in the I segment and at 12 h in the D1 segment (Fig. 5*A*, *top*). Intracellular signaling following cytokine receptor activation should increase c-fos, NFκB, and NGFI-A mRNAs; these patterns are observed in our assays (Fig. 5*A*, *middle*). ICAM-1 and SOCS-3, genes stimulated by inflammation, exhibited similar peaks with prolonged elevation in the I segment (Fig. 5*A*, *bottom*). Likewise, we found rises of heat-shock protein (HSP) mRNA, which is known to respond to activation of the hsf transcription factor. Activation of hsf also represses transcription of IL-1β mRNA (7). These patterns can be clearly seen in our hierarchical clustering (Fig. 3) and self-organizing maps (*cluster 0*; Fig. 3). These observations depict a complex inflammatory cascade following contusion. Genes in this cascade can be targeted for anti-inflammatory therapies that may be more specific and efficacious for acute SCI than standard methylprednisolone treatment (5).

Many of the mRNA changes at the impact site are consistent with neuronal loss. A recent histological study of SCI supports this neuron-specific loss (18). Using a similar rat contusion model, the number of appropriately stained astrocytes, oligodendrocytes, and neurons in the ventral spinal cord were determined at various times and at various distances from

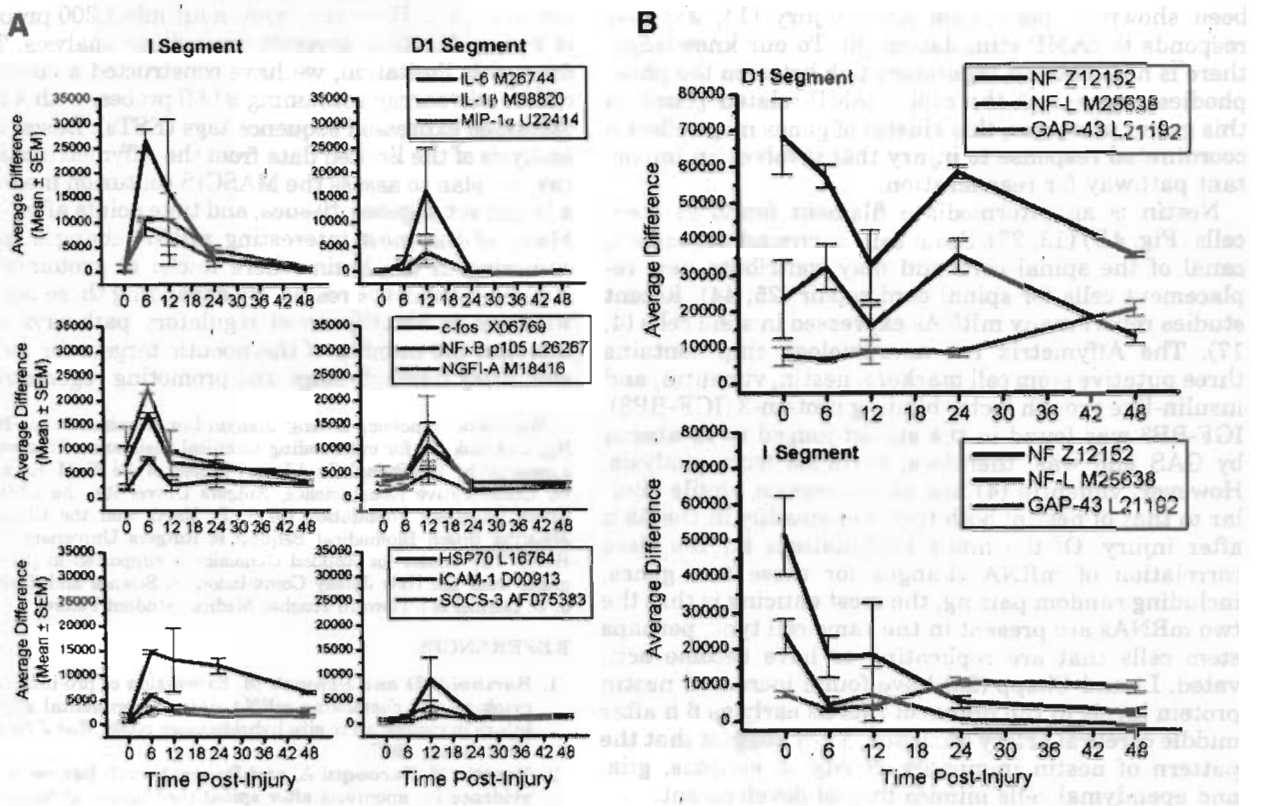

Fig. 5. *A*: inflammatory signaling mRNAs in I segment and D1 segment. Genes known to be involved in inflammatory signaling were plotted from the impact segment (*left*) and distal segment (*right*). *Top*: the temporal gene expression profiles of inflammatory cytokines. *Middle*: transcription factors. *Bottom*: inflammatory responses. All profiles shown have at least one time point that differed from control by ANOVA and the Duncan post-hoc test at 95% confidence levels. *B*: GAP-43 mRNA differs from that of other neuronal transcripts. Two neurofilament mRNAs demonstrate declining levels characteristic of many neuron-specific mRNAs. In contrast, GAP-43 mRNA levels in both the impact and distal segments rise over the 48 h following injury. All profiles shown have at least two time points that differed from control by ANOVA using the Duncan post-hoc test at 95% confidence levels.

the lesion center. The injury rapidly destroys ventral motor neurons (VMNs). By 4 h after injury, the 2.5- to 3.0-mm segment of cord around the epicenter lacked any intact VMNs. By contrast, only 20–25% of glial cells were lost, and the number of glial cells stayed constant at later time points. VMNs in the surrounding spinal cord continued to die over time, however. By 24 h, the length of cord devoid of VMNs increased to 4 mm. These observations strongly support the patterns of neuronal loss suggested by our microarray results.

We used the anchor gene clustering method to identify neuronal markers that exhibit a temporal pattern most like intermediate-weight neurofilament, a commonly-used neuron-specific marker (Fig. 4*B*). Two other neurofilaments (heavy and light chain), SNAP-25B and synaptic vesicle protein 2A (two synaptic proteins), and a cAMP phosphodiesterase matched the temporal profile of intermediate-weight neurofilament. The close correlation with these other putative neuronal markers supports the hypothesis that contusion causes a selective loss of neurons, rather than changes in mRNA synthesis or degradation. Interestingly, GAP-43 expression, which is associated with growing neurons, increased in both I and D1 segments. This suggests early activation of regeneration-associated genes in the acute period of injury. However, some reports suggest that GAP-43 expression may be glial under some circumstances (48). In situ hybridizations will be necessary to determine whether GAP-43 mRNA is expressed by neurons or glia.

Another gene that may influence early neurite outgrowth is PDE4, a phosphodiesterase (Fig. 4*A*). Recent work has identified cAMP as a critical regulator of neuronal growth in the presence of inhibitory molecules such as myelin-associated glycoprotein. PDE4 breaks down cAMP in neurons, and inhibition of PDE4 strongly stimulates axonal growth by increasing cAMP levels (8, 9). Our data show the injury markedly increases PDE4 expression by 6 h, and this expression closely correlates with another cAMP phosphodiesterase. Other genes associated with cAMP signaling also correlate with PDE4. These include activity and neurotransmitter-induced gene 6 (ania-6) and c-fos. Ania-6 and other members of the ania family are transcriptionally regulated by cAMP response element binding protein (CREB) (3). c-Fos expression has previously

been shown to peak soon after injury (14, 21) and responds to cAMP stimulation (6). To our knowledge, there is no identified regulatory link between the phosphodiesterases and the other cAMP-related genes in this group. However, this cluster of genes may reflect a coordinated response to injury that involves an important pathway for regeneration.

Nestin is an intermediate filament found in stem cells (Fig. 4*D*) (13, 27). Stem cells surround the central canal of the spinal cord and may contribute new replacement cells for spinal cord repair (25, 44). Recent studies report many mRNAs expressed in stem cells (4, 17). The Affymetrix rat neurobiology chip contains three putative stem cell markers: nestin, vimentin, and insulin-like growth factor binding protein-3 (IGF-BP3). IGF-BP3 was found in the subset judged to be absent by GAS and was, therefore, excluded from analysis. However, vimentin (4) has an expression profile similar to that of nestin; both increase steadily in the 48 h after injury. Of the many explanations for the close correlation of mRNA changes for these two genes, including random pairing, the most enticing is that the two mRNAs are present in the same cell type, perhaps stem cells that are replicating or have become activated. Li and Chopp (28) have found increased nestin protein levels in the brains of rats as early as 6 h after middle cerebral artery occlusion. They suggest that the pattern of nestin immunoreactivity in neurons, glia, and ependymal cells mimics that of development.

Finally, we chose a gene whose role has not been studied in SCI, GdNPF, to anchor temporal patterns in Fig. 4*C*. GdNPF is a serine protease inhibitor with neurite-promoting activity in chick sympathetic neurons (55), rat hippocampal neurons (16), and mouse neuroblastoma cells (43). Although the expression level of this gene after peripheral nerve lesion is variable (37), the protein is expressed for over 1 yr in a rat model of transient cerebral ischemia (24). Anchor cluster analysis revealed several interesting and unexpected genes. The mRNA that correlated best with GdNPF was COMT, the enzyme that catalyzes the degradation of catecholamines. COMT is of interest because of the role of norepinephrine in SCI. Rats that have been depleted of norepinephrine-producing cells showed less edema and better recovery from contusion injury than nondepleted animals (54). Similarly, an α_1-adrenergic blocker reduces edema and increases blood flow in injured spinal cord (47). Finally, interleukin-1β converting enzyme, also known as caspase 1, a pro-apoptotic signal (22), was part of the GdNPF cluster. Thus this cluster represents several functions that have not been studied in SCI models, and our results suggest that their role should be considered. The finding of increased COMT, along with a wealth of pharmaceutical data on regulation of COMT activity, suggests new therapeutic targets.

These results demonstrate the usefulness of microarrays to measure changes in gene expression after SCI. Distinct patterns of mRNA changes were observed, and these could be correlated with well-understood biological phenomena, including an immediate stress and inflammatory response, and a selective loss of neurons at the site of impact. However, examining only 1,200 probes, all of known function, severely limited our analysis. To address this limitation, we have constructed a custom rat cDNA microarray containing 9,660 probes, with 41% unidentified expressed sequence tags (ESTs). Based on our analysis of the limited data from the Affymetrix microarray, we plan to assess the MASCIS contusion model with a larger set of genes, tissues, and time points after injury. Many of the most interesting mRNA changes may be occurring in the brain where nuclei of axotomized descending pathways reside. By expanding these analyses, we hope to identify novel regulatory pathways and to increase the number of therapeutic targets for reducing secondary tissue damage and promoting regeneration.

We thank Wencheng Huang, Jianjun Liu, Darshan Desai, Bor Tom Ng, and Hok Ng for outstanding technical assistance. This work was supported by The Spinal Cord Injury Project of the W. M. Keck Center for Collaborative Neuroscience, Rutgers University, the Christopher Reeve Paralysis Foundation (to R. P. Hart), and the Charles and Johanna Busch Biomedical Bequest of Rutgers University (to R. P. Hart). The Center for Applied Genomics is supported in part with a grant from the New Jersey Commission on Science and Technology. J. B. Carmel is a Howard Hughes Medical Student Fellow.

REFERENCES

1. **Bartholdi D and Schwab M.** Expression of pro-inflammatory cytokine and chemokine mRNA upon experimental spinal cord injury in mouse: an in situ hybridization study. *Eur J Neurosci* 9: 1422–1438, 1997.
2. **Beattie M, Farooqui A, and Bresnahan J.** Review of current evidence for apoptosis after spinal cord injury. *J Neurotrauma* 17: 915–925, 2000.
3. **Berke J, Paletzki R, Aronson G, Hyman S, and Gerfen C.** A complex program of striatal gene expression induced by dopaminergic stimulation. *J Neurosci* 18: 5301–5310, 1998.
4. **Boyne L, Fischer I, and Shea T.** Role of vimentin in early stages of neuritogenesis in cultured hippocampal neurons. *Int J Dev Neurosci* 14: 739–748, 1996.
5. **Bracken M, Shepard M, Holford T, Leo-Summers L, Aldrich E, Fazl M, Fehlings M, Herr D, Hitchon P, Marshall L, Nockels R, Pascale V, Perot P, Piepmeier J, Sonntag V, Wagner F, Wilberger J, Winn H, and Young W.** Administration of methylprednisolone for 24 or 48 hours or tirilazad mesylate for 48 hours in the treatment of acute spinal cord injury. Results of the Third National Acute Spinal Cord Injury Randomized Controlled Trial National Acute Spinal Cord Injury Study. *JAMA* 277: 1597–1604, 1997.
6. **Bravo R, Neuberg M, Burckhardt J, Almendral J, Wallich R, and Muller R.** Involvement of common and cell type-specific pathways in c-fos gene control: stable induction of cAMP in macrophages. *Cell* 48: 251–260, 1987.
7. **Cahill C, Lin H, Price B, Bruce J, and Calderwood S.** Potential role of heat shock transcription factor in the expression of inflammatory cytokines. *Adv Exp Med Biol* 400B: 625–630, 1997.
8. **Cai D, Qiu J, Cao Z, McAtee M, Bregman BS, and Filbin MT.** Neuronal cyclic AMP controls the developmental loss in ability of axons to regenerate. *J Neurosci* 21: 4731–4739, 2001.
9. **Cai D, Shen Y, De Bellard M, Tang S, and Filbin M.** Prior exposure to neurotrophins blocks inhibition of axonal regeneration by MAG and myelin via a cAMP-dependent mechanism. *Neuron* 22: 89–101, 1999.
10. **Chee M, Yang R, Hubbell E, Berno A, Huang X, Stern D, Winkler J, Lockhart D, Morris M, and Fodor S.** Accessing genetic information with high-density DNA arrays. *Science* 274: 610–614, 1996.
11. **Citron B, Arnold P, Sebastian C, Qin F, Malladi S, Ameenuddin S, Landis M, and Festoff B.** Rapid upregulation of caspase-3 in rat spinal cord after injury: mRNA, protein, and cellular localization correlates with apoptotic cell death. *Exp Neurol* 166: 213–226, 2000.

12. **Constantini S and Young W.** The effects of methylprednisolone and the ganglioside GM1 on acute spinal cord injury in rats. *J Neurosurg* 80: 97–111, 1994.
13. **Dahlstrand J, Lardelli M, and Lendahl U.** Nestin mRNA expression correlates with the central nervous system progenitor cell state in many, but not all, regions of developing central nervous system. *Brain Res Dev Brain Res* 84: 109–129, 1995.
14. **Del-Bel E, Borges C, Defino H, and Guimaraes F.** Induction of Fos protein immunoreactivity by spinal cord contusion. *Braz J Med Biol Res* 33: 521–528, 2000.
15. **Eisen M, Spellman P, Brown P, and Botstein D.** Cluster analysis and display of genome-wide expression patterns. *Proc Natl Acad Sci USA* 95: 14863–14868, 1998.
16. **Farmer L, Sommer J, and Monard D.** Glia-derived nexin potentiates neurite extension in hippocampal pyramidal cells in vitro. *Dev Neurosci* 12: 73–80, 1990.
17. **Geschwind D, Ou J, Easterday M, Dougherty J, Jackson R, Chen Z, Antoine H, Terskikh A, Weissman I, Nelson S, and Kornblum H.** A genetic analysis of neural progenitor differentiation. *Neuron* 29: 325–339, 2001.
18. **Grossman S, Rosenberg L, and Wrathall J.** Temporal-spatial pattern of acute neuronal and glial loss after spinal cord contusion. *Exp Neurol* 168: 273–282, 2001.
19. **Grossman S, Wolfe B, Yasuda R, and Wrathall J.** Alterations in AMPA receptor subunit expression after experimental spinal cord contusion injury. *J Neurosci* 19: 5711–5720, 1999.
20. **Grossman S, Wolfe B, Yasuda R, and Wrathall J.** Changes in NMDA receptor subunit expression in response to contusive spinal cord injury. *J Neurochem* 75: 174–84, 2000.
21. **Hayashi M, Ueyama T, Nemoto K, Tamaki T, and Senba E.** Sequential mRNA expression for immediate early genes, cytokines, and neurotrophins in spinal cord injury. *J Neurotrauma* 17: 203–218, 2000.
22. **Hayashi T, Sakurai M, Abe K, Sadahiro M, Tabayashi K, and Itoyama Y.** Apoptosis of motor neurons with induction of caspases in the spinal cord after ischemia. *Stroke* 29: 1007–1012, 1998.
23. **Ho L, Guo Y, Spielman L, Petrescu O, Haroutunian V, V, Purohit D, Czernik A, Yemul S, Aisen P, Mohs R, and Pasinetti G.** Altered expression of a-type but not b-type synapsin isoform in the brain of patients at high risk for Alzheimer's disease assessed by DNA microarray technique. *Neurosci Lett* 298: 191–194, 2001.
24. **Hoffmann M, Nitsch C, Scotti A, Reinhard E, and Monard D.** The prolonged presence of glia-derived nexin, an endogenous protease inhibitor, in the hippocampus after ischemia-induced delayed neuronal death. *Neuroscience* 49: 397–408, 1992.
25. **Horner P, Power A, Kempermann G, Kuhn H, Palmer T, Winkler J, Thal L, and Gage F.** Proliferation and differentiation of progenitor cells throughout the intact adult rat spinal cord. *J Neurosci* 20: 2218–2228, 2000.
26. **Kwo S, Young W, and Decrescito V.** Spinal cord sodium, potassium, calcium, and water concentration changes in rats after graded contusion injury. *J Neurotrauma* 6: 13–24, 1989.
27. **Lendahl U, Zimmerman L, and McKay R.** CNS stem cells express a new class of intermediate filament protein. *Cell* 60: 585–595, 1990.
28. **Li Y and Chopp M.** Temporal profile of nestin expression after focal cerebral ischemia in adult rat. *Brain Res* 838: 1–10, 1999.
29. **Liebl D, Huang W, Young W, and Parada L.** Regulation of Trk receptors following contusion of the rat spinal cord. *Exp Neurol* 167: 15–26, 2001.
30. **Lipshutz R, Fodor S, Gingeras T, and Lockhart D.** High density synthetic oligonucleotide arrays. *Nat Genet* 21: 20–24, 1999.
31. **Lockhart D, Dong H, Byrne M, Follettie M, Gallo M, Chee M, Mittmann M, Wang C, Kobayashi M, Horton H, and Brown E.** Expression monitoring by hybridization to high-density oligonucleotide arrays. *Nat Biotechnol* 14: 1675–1680, 1996.
32. **Lomax M, Huang L, Cho Y, Gong T, and Altschuler R.** Differential display and gene arrays to examine auditory plasticity. *Hear Res* 147: 293–302, 2000.
33. **Lou J, Lenke L, Xu F, and O'Brien M.** In vivo Bcl-2 oncogene neuronal expression in the rat spinal cord. *Spine* 23: 517–523, 1998.
34. **McTigue D, Tani M, Krivacic K, Chernosky A, Kelner G, Maciejewski D, Maki R, Ransohoff R, and Stokes B.** Selective chemokine mRNA accumulation in the rat spinal cord after contusion injury. *J Neurosci Res* 53: 368–376, 1998.
35. **Metz G, Curt A, van de Meent Klusman I, Schwab M, and Dietz V.** Validation of the weight-drop contusion model in rats: a comparative study of human spinal cord injury. *J Neurotrauma* 17: 1–17, 2000.
36. **Mirnics K, Middleton F, Marquez A, Lewis D, and Levitt P.** Molecular characterization of schizophrenia viewed by microarray analysis of gene expression in prefrontal cortex. *Neuron* 28: 53–67, 2000.
37. **Niclou S, Suidan H, Pavlik A, Vejsada R, and Monard D.** Changes in the expression of protease-activated receptor 1 and protease nexin-1 mRNA during rat nervous system development and after nerve lesion. *Eur J Neurosci* 10: 1590–1607, 1998.
38. **Rajeevan M, Vernon S, Taysavang N, and Unger E.** Validation of array-based gene expression profiles by real-time (kinetic) RT-PCR. *J Mol Diagn* 3: 26–31, 2001.
39. **Ray S, Matzelle D, Wilford G, Hogan E, and Banik N.** Increased calpain expression is associated with apoptosis in rat spinal cord injury: calpain inhibitor provides neuroprotection. *Neurochem Res* 25: 1191–1198, 2000.
40. **Ririe K, Rasmussen R, and Wittwer C.** Product differentiation by analysis of DNA melting curves during the polymerase chain reaction. *Anal Biochem* 245: 154–160, 1997.
41. **Satake K, Matsuyama Y, Kamiya M, Kawakami H, Iwata H, Adachi K, and Kiuchi K.** Nitric oxide via macrophage iNOS induces apoptosis following traumatic spinal cord injury. *Brain Res Mol Brain Res* 85: 114–122, 2000.
42. **Schnell L, Fearn S, Schwab M, Perry V, and Anthony D.** Cytokine-induced acute inflammation in the brain and spinal cord. *J Neuropathol Exp Neurol* 58: 245–254, 1999.
43. **Shea T.** Transient neuritogenesis in NB2a/d1 neuroblastoma cells induced by glial-derived protease inhibitors. *Cell Biol Int Rep* 15: 437–443, 1991.
44. **Shihabuddin L, Horner P, Ray J, and Gage F.** Adult spinal cord stem cells generate neurons after transplantation in the adult dentate gyrus. *J Neurosci* 20: 8727–8735, 2000.
45. **Streit W, Semple-Rowland S, Hurley S, Miller R, Popovich P, and Stokes B.** Cytokine mRNA profiles in contused spinal cord and axotomized facial nucleus suggest a beneficial role for inflammation and gliosis. *Exp Neurol* 152: 74–87, 1998.
46. **Tamayo P, Slonim D, Mesirov J, Zhu Q, Kitareewan S, Dmitrovsky E, Lander E, and Golub T.** Interpreting patterns of gene expression with self-organizing maps: methods and application to hematopoietic differentiation. *Proc Natl Acad Sci USA* 96: 2907–2912, 1999.
47. **Uehara H.** Role of endogenous norepinephrine and effects of alpha- and beta-blockers in experimental spinal cord compression injury [in Japanese, with English abstract]. *Nippon Seikeigeka Gakkai Zasshi* 62: 1011–1018, 1988.
48. **Vitkovic L.** GAP-43 expression in macroglial cells: potential functional significance. *Perspect Dev Neurobiol* 1: 39–43, 1992.
49. **Wang C, Olschowka J, and Wrathall J.** Increase of interleukin-1β mRNA and protein in the spinal cord following experimental traumatic injury in the rat. *Brain Res* 759: 190–196, 1997.
50. **Whitney L, Becker K, Tresser N, Caballero-Ramos C, Munson P, Prabhu V, Trent J, McFarland H, and Biddison W.** Analysis of gene expression in multiple sclerosis lesions using cDNA microarrays. *Ann Neurol* 46: 425–428, 1999.
51. **Wittwer C, Herrmann M, Moss A, and Rasmussen R.** Continuous fluorescence monitoring of rapid cycle DNA amplification. *Biotechniques* 22: 130–138, 1997.
52. **Xu J, Fan G, Chen S, Wu Y, Xu X, and Hsu C.** Methylprednisolone inhibition of TNFα expression and NF-κB activation after spinal cord injury in rats. *Brain Res Mol Brain Res* 59: 135–142, 1998.
53. **Yan P, Xu J, Li Q, Chen S, Kim G, Hsu C, and Xu X.** Glucocorticoid receptor expression in the spinal cord after traumatic injury in adult rats. *J Neurosci* 19: 9355–9363, 1999.
54. **Yoshino S and Yone K.** Role of norepinephrine and excitatory amino acids in edema of the spinal cord after experimental compression injury in rats. *J Orthop Sci* 3: 54–59, 1998.
55. **Zurn A, Nick H, and Monard D.** A glia-derived nexin promotes neurite outgrowth in cultured chick sympathetic neurons. *Dev Neurosci* 10: 17–24, 1988.